



PAPER • OPEN ACCESS

## Mechanisms leading to plasma activated water high in nitrogen oxides

To cite this article: F Matějka *et al* 2023 *Phys. Scr.* **98** 045619

View the [article online](#) for updates and enhancements.

### You may also like

- [Development of poly \(1,8 octanediol-co-citrate\) and poly \(acrylic acid\) nanofibrous scaffolds for wound healing applications](#)  
Allison Goins, Vidhya Ramaswamy, Elliott Dirr et al.
- [A Predictive Thermodynamic-Based Model for Proton Conductivity of Proton Exchange Membranes Based on Poly\(Benzimidazole\)/Poly\(Acrylic Acid\) Blend](#)  
Zohre Taherkhani, Mahdi Abdollahi and Alireza Sharif
- [High Performance Arsenic: Multiwall Carbon Nanotube Composite Anodes for Li-Ion Batteries](#)  
Kevin A. Hays, Nathan A. Banek and Michael J. Wagner



## PAPER

## OPEN ACCESS

RECEIVED  
24 October 2022REVISED  
14 January 2023ACCEPTED FOR PUBLICATION  
15 March 2023PUBLISHED  
28 March 2023

Original content from this work may be used under the terms of the [Creative Commons Attribution 4.0 licence](#).

Any further distribution of this work must maintain attribution to the author(s) and the title of the work, journal citation and DOI.



# Mechanisms leading to plasma activated water high in nitrogen oxides

F Matějka<sup>1,2</sup> , P Galář<sup>2,\*</sup> , J Khun<sup>1</sup>, V Scholtz<sup>1</sup> and K Kůsová<sup>2</sup> <sup>1</sup> University of Chemistry and Technology, Technická 3, Prague, Czech Republic<sup>2</sup> Institute of Physics, Czech Academy of Sciences, Cukrovarnická 10, Prague 6, Czech Republic

\* Author to whom any correspondence should be addressed.

E-mail: [galar@fzu.cz](mailto:galar@fzu.cz)**Keywords:** plasma activated water, non-thermal plasma, mechanisms of nanoparticles surface modifications, plasma-liquid phase interaction

## Abstract

Plasma activated water (PAW) is a unique highly reactive medium, traditionally used in medicine and agriculture because of its decontamination and disinfection abilities. Recently, we have shown that this medium can also be beneficial for tailoring the surface chemistry of semiconductor nanostructures if its composition is tuned to contain a high concentration of nitrogen-related species (HiN:PAW). However, pathways leading to the production of HiN:PAW remained unclear, which we address in this article. By monitoring the composition of the produced PAW and the concentration of selected species in the discharge under different activation geometries and discharge conditions, we identify the activation geometries favourable for the production of HiN:PAW using two phenomenological factors, a barrier parameter  $P$  and a maximum effective radius of the vessel  $r_{\max}$ . A key point is the presence of a barrier area in the discharge reactor, which forms as a result of the favourable activation geometry and a discharge with prevailing more reactive atomic species. This area acts as a partial barrier between the discharge and the surrounding air atmosphere, limiting, but still allowing a flow of source  $N_2$  molecules from the surrounding atmosphere. The minimal and ideal build-up times of 10 and 30 min, respectively, for the discharge to stabilize are also reported. Using the reported experimental settings, we were able to produce HiN:PAW containing a mixture of various reactive species beneficial for the surface modification of nanoparticles, with the  $NO_3^-$  to  $H_2O_2$  ratio of at least  $20 \times 10^3:1$ , in contrast to approximately 1:1 under more traditional conditions.

## 1. Introduction

Non-thermal plasma (NTP) is a cutting-edge technology which has been gaining momentum during the last decade due to the simple design of the necessary apparatus, its ease of use, cost-effective operation and a general lack of toxic effects. NTP is generated under specific conditions, when the energy from the plasma source is transferred mainly to electrons in the discharge [1, 2], which then turns electrons into high-energy charge carriers (several eV,  $\sim 10$  kK), while the positive ions and neutral molecules making up most of the mass are kept at almost ambient temperature. Thus, in contrast to other types of treatment, the interaction with NTP does not cause thermal damage, even though it still can affect materials through a wide range of reactive species originating in the atmosphere where the discharge burns. Many different ways to generate NTP by electric discharges were introduced in the last decades [3], mainly with the aim of treating bio-objects [4–8]. They vary in the structure of electrodes, the type of power sources, a pulse/continual regime and the composition of the used atmosphere. Thanks to these techniques, NTP was successfully employed in a wide range of applications, starting from rendering surfaces hydrophilic [9], their decontamination [10], antifungal and conservation treatment of food and seeds causing extension of their shelf life [8, 11–13] and green technology [14] for the effective disinfection of respirators and other medical equipment [15, 16].

An important example of the use of NTP are plasma activated liquids [1, 17]. In plasma activated liquids, the interaction of reactive species and high-energy electrons in NTP with the liquid results in a specific chemical composition of the NTP-treated, so-called activated liquid [18–20]. Naturally, the most common activated liquid is water [1, 17, 21]. Plasma activated water (PAW) contains many short-lived and long-lived reactive species. A few hundreds of possible chemical pathways related to NTP and PAW generation were described [1, 17, 22]. The typical most abundant short-lived species are ozone  $O_3$ , nitric oxide (NO) or peroxyntrous acid (ONOOH), long-lived species are most commonly represented by hydrogen peroxide ( $H_2O_2$ ), followed by nitrites and nitrates ( $NO_2^-$  and  $NO_3^-$ ) [23]. However, the real relevance of the reactions depends on many parameters such as the used NTP system, surrounding conditions, continual/pulsed excitation regime, etc [20, 21, 23]. As a result of its composition, PAW is an environment very hostile to microorganisms, making it an ideal material for the above-mentioned decontamination and disinfection applications.

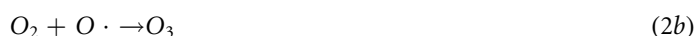
The plasma activation of water is based on the interaction of molecules and other particles from the surrounding gas and plasma burning in the gas with the liquid phase. Usually, the discharge is located in the gas phase and at the gas-liquid interface. High-speed electrons from the discharge react with molecules of the gas causing their dissociation, when it burns in air, the discharge creates mainly oxygen (dissociation energy of  $O_2$  - 5.2 eV molecule<sup>-1</sup>) and nitrogen radicals ( $N_2$ , 9.8 eV molecule<sup>-1</sup>) [23]:



Due to high dissociation energy of the nitrogen molecule, nitrogen radicals can be effectively created also through the reaction of nitrogen molecule with oxygen radicals [23]:



In the discharge area, further reactions leading to radicals and other species are in progress, yielding mostly  $H_2O_2$ , nitrogen-related species (NO,  $HNO_2$ ,  $NO_2$ ) and ozone [24]:



In the liquid phase, the produced  $H_2O_2$  can then be consumed by [24]:



More detailed list of chemical reactions related to discharge burning at ambient conditions, at the air/liquid interface and inside the liquid can be found elsewhere [23–25].

In nanomaterials, surface chemistry plays an important role in their physical and chemical properties, such as light generation efficiency, surface reactivity, dispersibility, toxicity, etc [26–28]. Countless surface-modification techniques are currently available [29–31]. Among these techniques, the surface modification in NTP and by plasma activated liquids is new and attractive due to its simplicity and low cost [18]. In one example, PAW was successfully applied to a nanostructured conductive polymer causing its homogenous oxidation [32]. The treated polymer then showed good stability and good conductive properties. The role of the surface is even more profound in semiconductor nanoparticles. The first pioneering works using PAW and plasma-activated ethanol applied to silicon nanocrystals showed a slight increase of their light generation efficiency and stability [18]. The limitation for further PAW applications to semiconductor nanocrystals was mainly the presence of  $H_2O_2$ , which easily degrades them and also neutralizes the prospective air-originating nitrogen reactive species [23, 33], which can be advantageous surface passivating agents.

In our previous work [34], we introduced a simple technique producing PAW with a high concentration of  $NO_x$  (HiN:PAW). This PAW has a novel and unique chemical composition, having only a marginal concentration of  $H_2O_2$  and, at the same time, extraordinarily high concentrations of nitrites and nitrates ( $NO_3^-$ : 80 000  $\mu M$ ), suitable for the surface passivation of semiconductor nanoparticles. The key for the generation of HiN:PAW was a combination of a particular NTP generation system (transient spark discharge) and the use of a closed or semi-closed container. In that work [34], the application of HiN:PAW to several types of semiconductor nanoparticles resulted in the enrichment of their surface layer with nitrogen-related species. Especially in the case of Si-NCs, this new termination caused a significant increase in their light generation efficiency and dispersibility and stability in water. Despite being clearly beneficial as a surface-modification agent, the detailed mechanisms leading to a PAW composition favourable for the surface modification of nanoparticles still remains unclear. Therefore, in this contribution, we focus on an in-depth study of the mechanisms leading to the production of HiN:PAW. We monitor the dynamics of the chemical composition of NTP and HiN:PAW under specific conditions (discharge properties, enclosure of the surrounding atmosphere

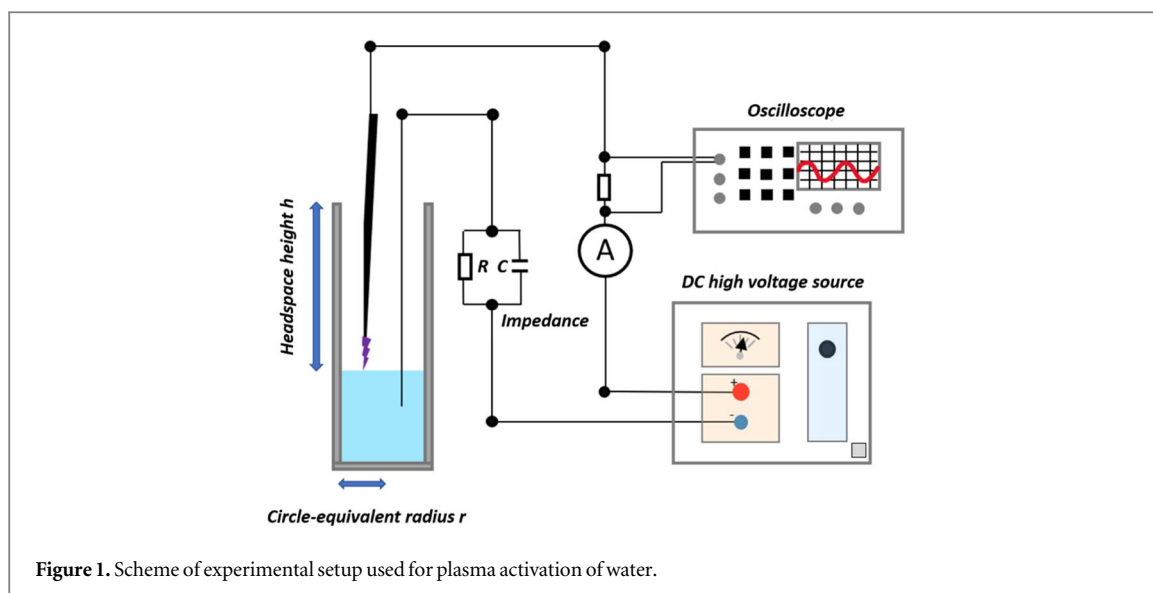


Figure 1. Scheme of experimental setup used for plasma activation of water.

etc). Based on these results and chemical reactions in atmospheric NTP, the NTP/water interface and the HiN:PAW itself, we propose a reaction model of conditions favourable for the generation of HiN:PAW. We highlight that the shape of the container, the amount of water, the discharge properties, dissociation of air related molecules and high humidity all play a significant role in the activation process. These results can be used not only for the further development of HiN:PAW generation systems, but can also serve as a guide in activation processes of other prospective liquids, whose application is as of now extremely rare.

## 2. Experimental

### 2.1. Transient spark discharge apparatus

The transient spark discharge in point-to-plane geometry is generated by a system consisted of a commercial high-voltage source (Utes Brno, DC source HT 2103) (max. voltage 10 kV), oscilloscope (Tektronix 2465, 300 MHz Oscilloscope), ammeter (analog, METRA BLANSKO DU 20), a stabilizing ballast impedance and two electrodes (figure 1). The point electrode is represented by a commercial surgical needle (Medoject,  $0.7 \times 40$  mm) and is connected to the positive pole of the power supply. The planar electrode is represented by the surface of the treated water which is connected by a platinum wire to the negative pole. The point electrode was localized 2.5 mm above the water surface. Therefore, the discharge burned between the upper electrode and the water level. The ballast impedance contains parallel connection of a  $10 \text{ M}\Omega$  resistor and capacitor system of adjustable overall capacity (0.05, 0.1, 0.25, 2.0 and 95.0 nF). The variation of the capacitance affected mainly the pulse peak current and pulse period, which varied from about 9 to 13 A and 300 to 500  $\mu\text{s}$ , respectively. The pulse duration was determined of approx. 30–50 ns. The discharge burnt in ambient conditions (room temperature, no humidity or atmosphere control was applied). Approximate average value of the discharge current measured by analogous ammeter was 500  $\mu\text{A}$  and supply voltage 9 kV. The current and voltage waveforms were published elsewhere [35]. The electrodes were inserted into various reactors. Three main ones were labelled as *Narrow*, *Medium* and *Wide*. The *Narrow* reactor was realized by a quartz cuvette of a  $1 \times 1 \times 4.3 \text{ cm}^3$  (without the airtight stopper wedge on the top), the *Medium* reactor by a 5 ml glass beaker of a 2.3 cm diameter and 3 cm tall, and the *Wide* reactor by a glass Petri dish of 4.3 cm diameter and 1 cm tall. The reactors were characterized using two parameters: headspace height  $h$  that defines the distance between edge of the reactor and the water level and the circle-equivalent radius  $r$  (effective radius) defined as  $r = (S/\pi)^{1/2}$ , where the  $S$  is area of reactor base (figure 1). To study the threshold conditions of HiN:PAW generations we also used standard glass vials of radius 0.65, 1.0 and 1.25 cm.

### 2.2. Plasma activation of water

Sufficient volume (1–3 ml) of deionized water was pipetted into the used reactors, the electrode system was adjusted and the water surface was exposed to the transient spark discharge for 30 min using ballast impedances of parameters as described above (figure 1). The properties of the discharge were monitored during the whole activation process. Even though evaporation was minimal during the activation, the water level was kept at the same position by adding water to the reactor ( $\sim 0.1$  ml during the whole activation process).

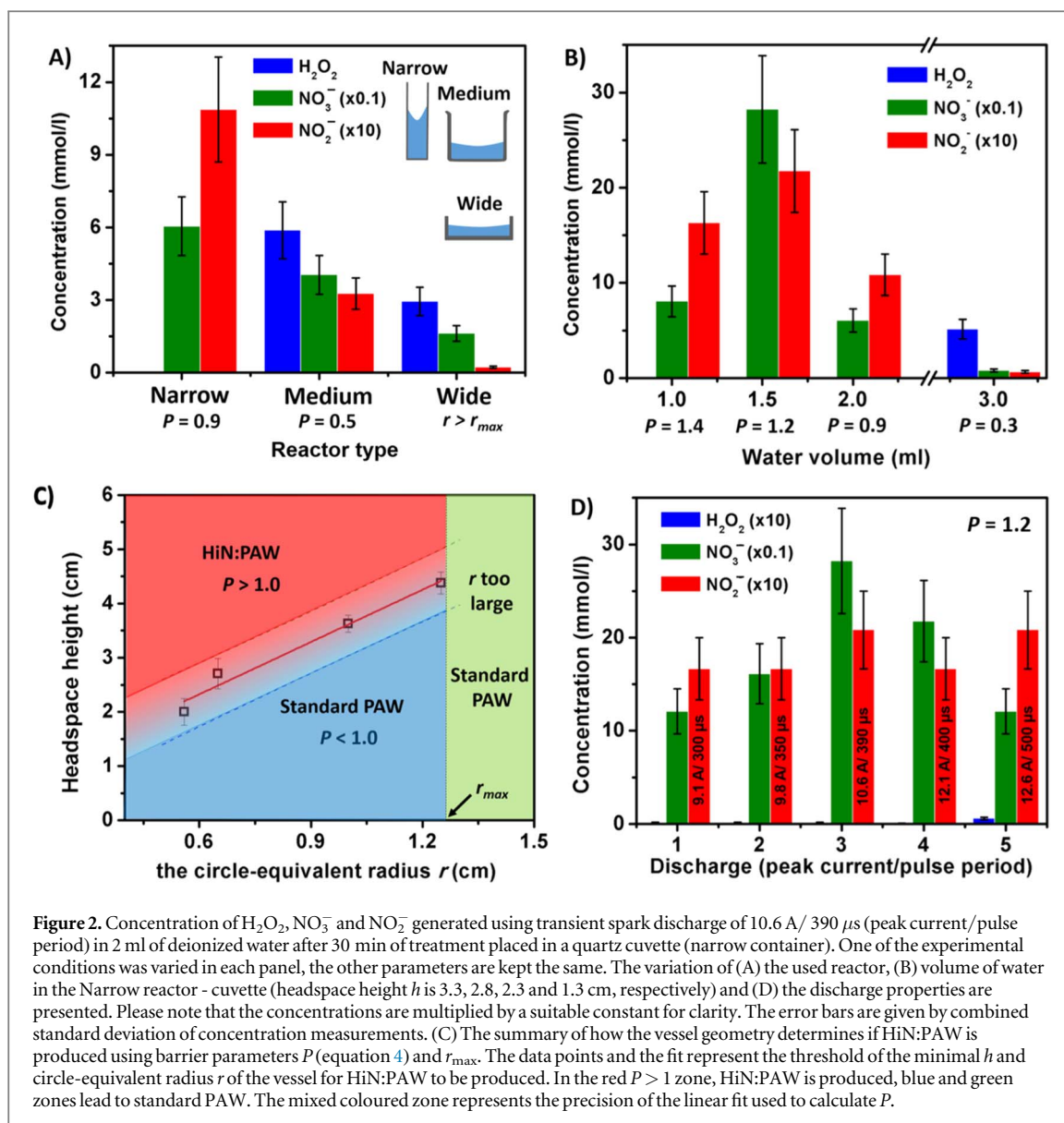


**Figure 2.** Concentration of  $H_2O_2$ ,  $NO_3^-$  and  $NO_2^-$  generated using transient spark discharge of 10.6 A / 390  $\mu$ s (peak current/pulse period) in 2 ml of deionized water after 30 min of treatment placed in a quartz cuvette (narrow container). One of the experimental conditions was varied in each panel, the other parameters are kept the same. The variation of (A) the used reactor, (B) volume of water in the Narrow reactor - cuvette (headspace height  $h$  is 3.3, 2.8, 2.3 and 1.3 cm, respectively) and (D) the discharge properties are presented. Please note that the concentrations are multiplied by a suitable constant for clarity. The error bars are given by combined standard deviation of concentration measurements. (C) The summary of how the vessel geometry determines if HiN:PAW is produced using barrier parameters  $P$  (equation 4) and  $r_{max}$ . The data points and the fit represent the threshold of the minimal  $h$  and circle-equivalent radius  $r$  of the vessel for HiN:PAW to be produced. In the red  $P > 1$  zone, HiN:PAW is produced, blue and green zones lead to standard PAW. The mixed coloured zone represents the precision of the linear fit used to calculate  $P$ .

### 2.3. Characterization of PAW concentration and discharge properties

Within the PAW composition, the  $H_2O_2$ ,  $NO_2^-$ ,  $NO_3^-$  species were monitored. The measurements were realized 5 min after finishing of the activation. The concentration of nitrates and nitrites were obtained using standard test strips Quantofix Nitrate/Nitrite (ref no. 91313), showing gradation as follows: 0, 10, 25, 50, 100, 250, 500  $mg\ l^{-1}$  for nitrates and 0, 1, 5, 10, 20, 40, 80  $mg\ l^{-1}$  for nitrites. To extend the concentration range beyond these values, PAW was diluted with distilled water from 10 to 1000 times. The concentration of hydrogen peroxide was characterized by test strips Quantofix Peroxide 25 (ref no. 91319) having gradation as follows: 0, 0.5, 2, 5, 10, 25  $mg\ l^{-1}$ . The concentration error was calculated based on the combined standard deviation composed of precision of used test strips and statistical error of repeated measurements. Ozone was not monitored, because its production is not significant while using the transient spark discharge system [36].

The linear fit in figure 2(C) was performed using Matlab 2015 b. Due to the small number of data points, the robust linear least-squares fitting method using bisquare weights was applied. The presented uncertainty gives the prediction observational bounds for one observation (non-simultaneous) for the 67% confidence level.

The NO and  $NO_2$  concentrations in discharge area were measured by Serinus 40H  $NO_x$  analyser, ACOEM Ecotech (NO and  $NO_2$  range up to 1000 ppm, measurement accuracy  $\pm 1\%$ , gas flow rate 0,16 slm) using chemiluminescence detection. Gas mixture for analysis was taken by Teflon tube of inner diameter 3 mm introduced into the cuvette or 5 ml beaker from two different positions. The first position was immediately at the suspension surface (ca 2 mm above the suspension surface), the second position was upper edge of the vessel (ca 13 mm above the suspension surface).

The emission spectra of the discharges were acquired using the Shamrock 300i spectrograph (Andor, Oxford Instruments) with an EMCCD camera (Newton 971, Andor, Oxford Instruments). The emission spectra at

specific times were not measured in the whole spectral range at once, but stepwise. The spectra were combined afterwards. The spectra were corrected for the sensitivity of the whole spectroscopic system. The discharge frequency and peak current were obtained from the oscilloscope as described elsewhere [35].

### 3. Results

In order to understand the mechanism of the generation of HiN:PAW, we first focus on how the experimental conditions influence the outcome of the activation processes in the liquid phase and then we move on to the gas phase and the properties of the discharge. The processes taking place above the water level and the chemical reactions in the water while it is being activated are closely interconnected and specific conditions need to be met in both these phases for HiN:PAW to be the product of the activation process.

#### 3.1. Influence of activation conditions on the reaction products in the liquid phase

Deionized water was plasma activated using pulsed transient spark discharge, the used apparatus and experimental conditions are described in detail in *Experimental section* and in figure 1. In order to understand the mechanism of the generation of HiN:PAW, the system used in our previous work [34] was employed. In particular, as a starting setting we used a narrow quartz cuvette containing 2 ml of distilled water, discharge conditions of 10.6 A/390  $\mu$ s (peak current/pulse period,  $R = 10 \text{ M}\Omega$ ,  $C = 0.25 \text{ nF}$ ) and the modification was realized for 30 min. We varied the reactor shape, the amount of the treated water and the properties of the discharge. To determine the composition of the produced PAW rather than focusing on the short-lived reactive, the measurements of  $\text{H}_2\text{O}_2$ ,  $\text{NO}_2^-$ ,  $\text{NO}_3^-$  concentrations were made 5 min after finishing the activation.

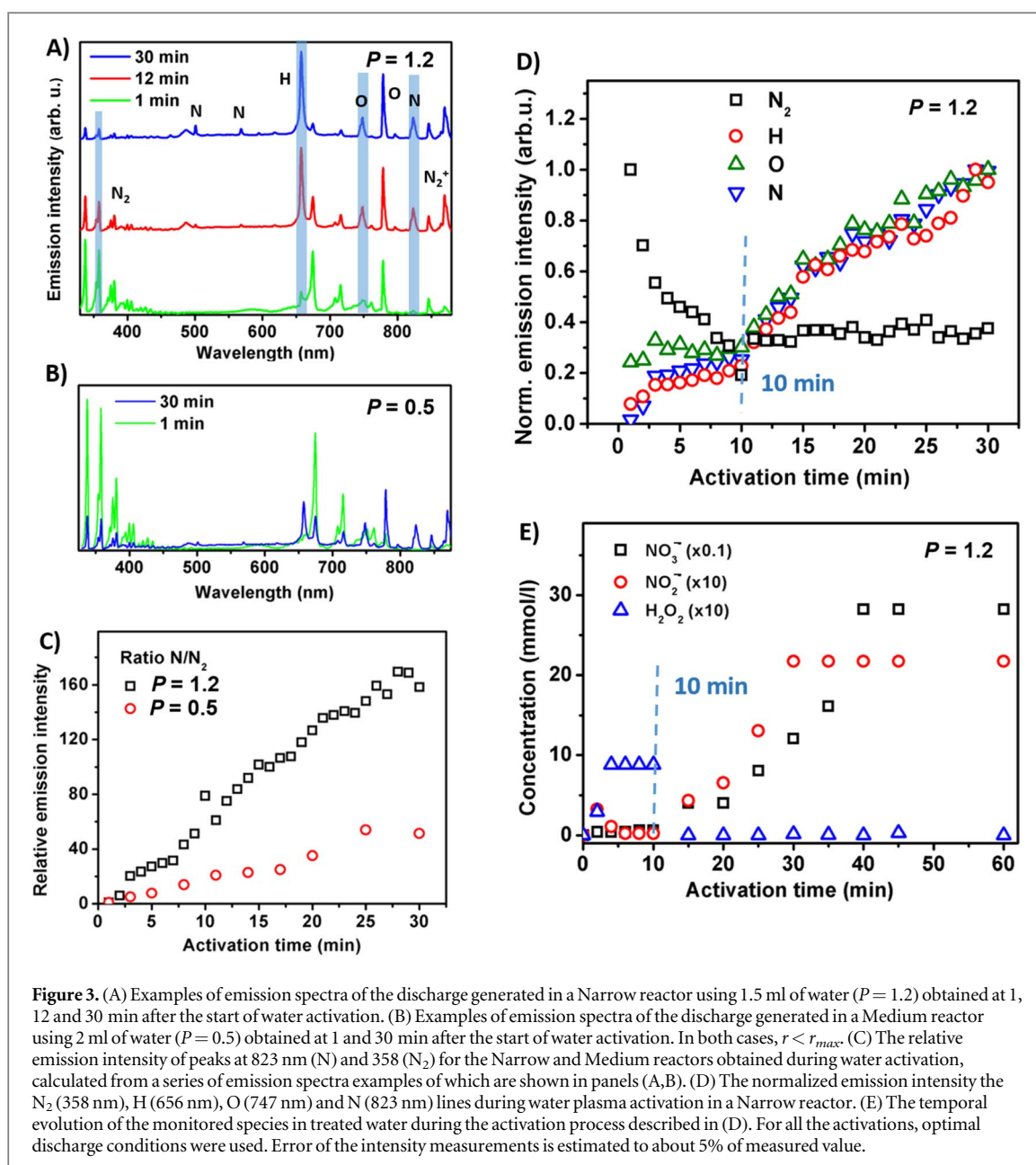
The geometry of the reactor can have a considerable impact on the local atmosphere around the discharge, therefore, on the reactants and on the rates in which reactions listed in equations (2a–2e) proceed. We used three different types of reactors with a significantly different degree of the separation of the discharge from the non-ionized surrounding atmosphere: (A) Narrow (quartz cuvette), (B) Medium (glass beaker) and (C) Wide (Petri dish). The reactors contained the same amount of water, 2.0 ml. The concentrations of the most important reactants in PAW ( $\text{H}_2\text{O}_2$ ,  $\text{NO}_2^-$ ,  $\text{NO}_3^-$ ) produced in reactors with different geometries are bar-plotted in figure 2(A). Clearly, only the Narrow reactor produced HiN:PAW because it yields the intended high concentration of nitrates and nitrites and at the same time a negligible amount of hydrogen when compared to the more open types of reactors. Thus, the more open space around the discharge clearly leads to the production of more  $\text{H}_2\text{O}_2$  and a decrease in the concentration of nitrogen-related radicals.

Using the reactor yielding the lowest concentration of hydrogen peroxide (the Narrow reactor), the next key parameter which alters the settings of the system is the volume of water in the reactor. On the one hand, an increase in the amount of water should decrease the concentration of plasma-generated reactive species after the 30-minute treatment, but, on the other hand, an opposite effect can also be expected. The more air (less water) is present in the reactor, the weaker the exchange of the reactive species from the discharge with the atmosphere outside the reactor is, impacting the discharge conditions and thus the generated reactive species in PAW. To investigate this trade-off, the volume of water in the cuvette was varied in the range between 1 ml (minimal possible amount) and 3 ml. Under these conditions, the distance of water surface from the cuvette edge (labelled as headspace height  $h$ ) varied from 3.3 to 1.3 cm. The composition of the PAW produced under these conditions was monitored, see figure 2(B). Settings with cuvettes holding a smaller volume of water led to the production of HiN:PAW, but the volume of 1.5 ml ( $h = 2.8 \text{ cm}$ ) was found to be optimal in terms of the produced composition. When the headspace height decreased to 1.3 cm (3 ml of water) during the plasma activation process, high concentration of  $\text{H}_2\text{O}_2$ , was produced, yielding PAW of a traditional chemical composition rather than HiN:PAW.

In order to generalize these findings, we repeated the experiment from figure 2(B) using another set of reaction vessels with different geometries. We carried out the water activation procedure with the volume of water in each vessel increased in steps and noted the critical volume above which the produced PAW reverted to high  $\text{H}_2\text{O}_2$  content. The results are presented as the dependence of headspace height  $h$  on the circle-equivalent radius of the vessel  $r$ , which well follows a linear dependence, see figure 2(C). Linear fit of this dependence allows us to phenomenologically formulate a dimensionless effective barrier parameter  $P$ , which characterizes how limited the exchange of the reactive species between the atmosphere and the discharge is. The barrier parameter  $P$  reads:

$$P = \frac{h \text{ (cm)} - 0.3823}{3.225r \text{ (cm)}} \quad (4)$$

where the prediction band for  $\Delta h$  is  $\Delta h = 0.555\sqrt{0.7354r^2 - 1.333r + 1.657}$ . For the experiment geometry to produce HiN:PAW, it is necessary that  $P > 1$ . We also observed that any vessel with the circle-equivalent radius



wider than 1.25 cm (labelled as  $r_{max}$ ) did not lead to HiN:PAW no matter what the headspace height was. Therefore, we separated the area of figure 3(c) to three zones: the red zone passing both necessarily conditions ( $P > 1$  and  $r < r_{max}$ ) for HiN:PAW generation, the blue one violating the first condition ( $P < 1$ ) and the green one violating the second condition (and  $r > r_{max}$ ). The multicolor overlap zones depict the uncertainties of the zone borders. The underlying physical mechanism behind these constraints is clearly the need for the discharge to burn in a limited (the  $r > r_{max}$  condition) and relatively isolated (the condition for  $h$  through the  $P$  parameter) volume to be able to produce local conditions favourable for the generation of HiN:PAW and act as an effective barrier. Thus, the barrier parameters  $P$  and  $r_{max}$  characterize the geometry of the experiment favourable for the production of HiN:PAW, and therefore, its value is included at each experiment in the text of this article (on one occasion in figure 2(A), PAW lacking hydrogen peroxide, but containing not ideal concentration of nitrides was detected even for  $P = 0.9$ , but this value is close enough to the  $P = 1$  threshold considering the experimental error). The value of  $r_{max}$  very likely depends on the radius of the discharge ( $r_d$ ). Using broader discharge while keeping its other properties the same can result in an increase in the  $r_{max}$  value. However, a change of  $r_d$  cannot be, in the case of transient spark, easily realized, therefore such a study is not included. To be complete, we present the value of a dimensionless parameter  $r_{max}/r_d$  which was about 23 in our experimental system, where the lateral size of the discharge (1.1 mm) was estimated using a long-exposure photograph.

The next relevant parameter is the characteristics of the transient spark itself. The delivery of energy is critical for the generation of radical species from molecules present in normal atmosphere, which affects the whole process of water activation. Figure 2(D) presents the concentrations of the species of interest as a function of a

variety of discharge conditions. In this activation process, the narrow reactor filled with 1.5 ml of water was used and the capacitance of the stabilizing ballast was possessed values of: 0.05, 0.1, 0.25, 2.0 and 95.0 nF, which resulted in changes in pulse peak current and period (9.1–12.6 A and 300–500  $\mu$ s, respectively). As shown in figure 2(D), the prolongation of the period of pulses leads mostly to changes in the concentrations of  $\text{NO}_3^-$  in the produced HiN:PAW. These concentrations first rise, but then start to decline for pulses longer than 390  $\mu$ s. At even longer pulse duration of more than 500  $\mu$ s, the concentration of  $\text{H}_2\text{O}_2$  starts to rise, marking the end of the range of conditions suitable for the production of HiN:PAW.

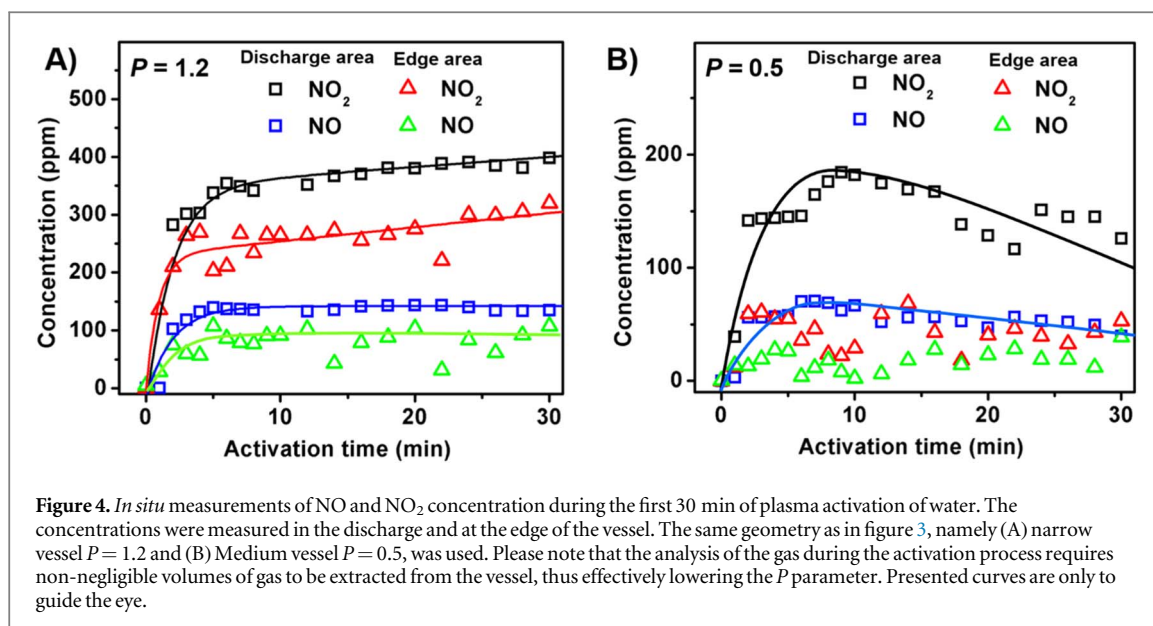
### 3.2. Influence of activation conditions on the reactive species in the discharge

Following from equations (1a–1c) and (2a–2c), the composition of the plasma also influences the final product. Thus, the composition of the plasma discharge was investigated for optimal conditions for the production of HiN:PAW, as detailed above. To fulfil this task, we selected a combination of emission spectroscopy and a direct chemical analysis using  $\text{NO}_x$  analyser. The former method allows us in a simple but precise way to compare how the ratios related to specific molecules/atoms evolve in time *in situ* when the discharge burns without affecting the conditions inside the reactor. However, it does not provide any quantification of the gas chemical composition during the activation, which is where the direct chemical analysis comes in. The disadvantage of the latter method is the fact that a part of the gas need to be extracted from the reactor area for the analysis, thus affecting the conditions in the reactor by effectively decreasing the barrier factor  $P$ . To compare the discharge leading to HiN:PAW and that producing the more traditional composition, we analysed the discharge in the Narrow reactor keeping  $P > 1$  ( $P = 1.2$ ) and the Medium reactor with  $P < 1$  ( $P = 0.5$ ) with  $r < r_{\max}$  in both cases.

The emission spectra were acquired at various times during the activation process and, simultaneously, the composition of the water while it was being activated was characterized, see figure 3. As expected from the activation process being carried out at ambient atmosphere, the species detected in the discharge under the  $P > 1$  condition include air-originating molecules and atoms  $\text{N}_2$ , N, H, O (figure 3(A)). During the first few minutes of the activation process, the molecular  $\text{N}_2$  signal decreased, which was accompanied by only a weak rise in the atomic signal (figure 3(D)). However, about 10–12 min after the discharge was switched on, there is clearly a qualitative instead of a simple quantitative change in the discharge, when it transforms from discharge containing mainly ionized molecules into the more energetic discharge containing their dissociated parts, implying more reactive species. Later in the activation process, the atomic peaks further rise and the molecular peaks are almost vanquished. The discharge stabilizes after about 30 min, which gives the timeframe necessary for the activation process of HiN:PAW to be completed. When  $P < 1$ , we also detected a decrease of the molecular  $\text{N}_2$  signal with time, but it was accompanied by only a mild rise of the atomic emission signal, which was insufficient for the discharge to significantly dissociate the air molecules. This difference is evident from figure 3(C), where we compared the dynamics of the ratio between the emission intensity of the N and  $\text{N}_2$  peaks for these two sets of experimental conditions.

In addition to the discharge, the composition of the produced PAW was monitored simultaneously with the emission spectroscopy ( $P > 1$ ) and the measured dynamics are compared in figures 3(D) and (E). Clearly, after the discharge was switched on, the gradual decrease in the molecular  $\text{N}_2$  signal in the emission spectrum is accompanied by an increase in  $\text{H}_2\text{O}_2$  and low of  $\text{NO}_3^-$  and  $\text{NO}_2^-$  content in the activated water, leading to the traditional high- $\text{H}_2\text{O}_2$  content. However, at later stages of the activation process, as the discharge stabilized and dissociated species (N) prevailed in the emission spectra, the rise of  $\text{NO}_3^-$  and  $\text{NO}_2^-$  in water was accompanied by a decrease in  $\text{H}_2\text{O}_2$  and further increase of the atomic N signal in the emission spectrum of the discharge. The transition between these two modes of operation occurred approximately 10 min after the discharge was switched on, giving the timeframe necessary for the discharge to stabilize. The dissociation of the air molecules in the discharge area is thus in correlation with the changes in the concentration of the monitored species in PAW and the presence of atoms in the discharge is clearly a necessary condition for the production of HiN:PAW.

A further corroboration of the presented findings was supported by direct *in situ* analysis of NO and  $\text{NO}_2$  concentration during plasma activation of water using the same two sets of experimental conditions (figure 4). As can be seen in figure 4(A) ( $P = 1.2$ ), the concentration of  $\text{NO}_x$  rose fast within the first approximately 10 min and, in case of the  $\text{NO}_2$ , then kept slowly increasing for the next 20 min in the discharge area. Qualitatively comparable results with somewhat lower concentrations and a higher spread between values were obtained at the edge of the vessel. These dynamics are in correlation with the one observed for the emission intensity of N using emission spectroscopy (figure 3), only the secondary rise at  $t > 10$  min is weaker. This difference is easily understandable, because during the analysis the discharge is disrupted by the gas extraction to the analyser, which effectively lowers the  $P$  parameter and prevents the ideal conditions for the production of HiN:PAW from stabilizing, effectively lowering the  $P$  parameter. Under the  $P = 0.5$  conditions (Medium vessel, figure 4(B)), the initial rise of the  $\text{NO}_x$  concentration in the discharge area within the first approximately 10 min also occurred. However, the concentration of both NO and  $\text{NO}_2$  was about 2 times lower and the initial rise is followed by



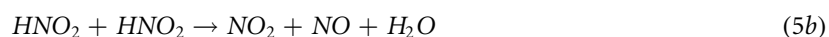
secondary decrease instead of a rise. Moreover, the concentration of both NO<sub>x</sub> was low and highly unstable at the edge of the vessel. Thus, it is evident that inside the vessel with  $P > 1$ , the generation of NO<sub>x</sub> is more effective and the conditions are favourable for a secondary rise of their concentration after the first 10 min during water activation in contrast to the vessel of  $P < 1$ , even though this quantitative method by design prevents the reaching of ideal conditions for the experiment. It is noteworthy that the  $P$  factor and the radius of the vessel did not affect the time period of initial rise, in both cases the initial rise was realized within about first 10 min.

## 4. Discussion

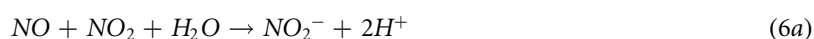
The chemical reactions from equations (1)–(3) are in progress in every PAW system and they represent the basic framework explaining the formation of nitrites/nitrates and hydrogen peroxide in PAW. However, by setting up certain conditions of the generating system, the rate at which the individual reactions happen will change significantly [23]. In this way, the final composition of PAW can be altered. As will be discussed in detail below, we propose that there are two key features of our system which lead to the production of HiN:PAW. These features are (i) the formation of a gas-discharge transition area, which governs the conditions of the discharge, and (ii) the discharge properties with prevailing atomic species and the existence of a higher-humidity area possibly with water microdroplets close to the water/discharge interface, which is favorable for the generation of nitrogen-related species. Both these processes clearly strongly depend on the geometry of the reaction vessel and the volume of the vessel occupied by water as well as on the discharge itself, as studied in figures 2 and 4.

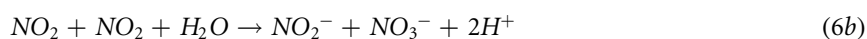
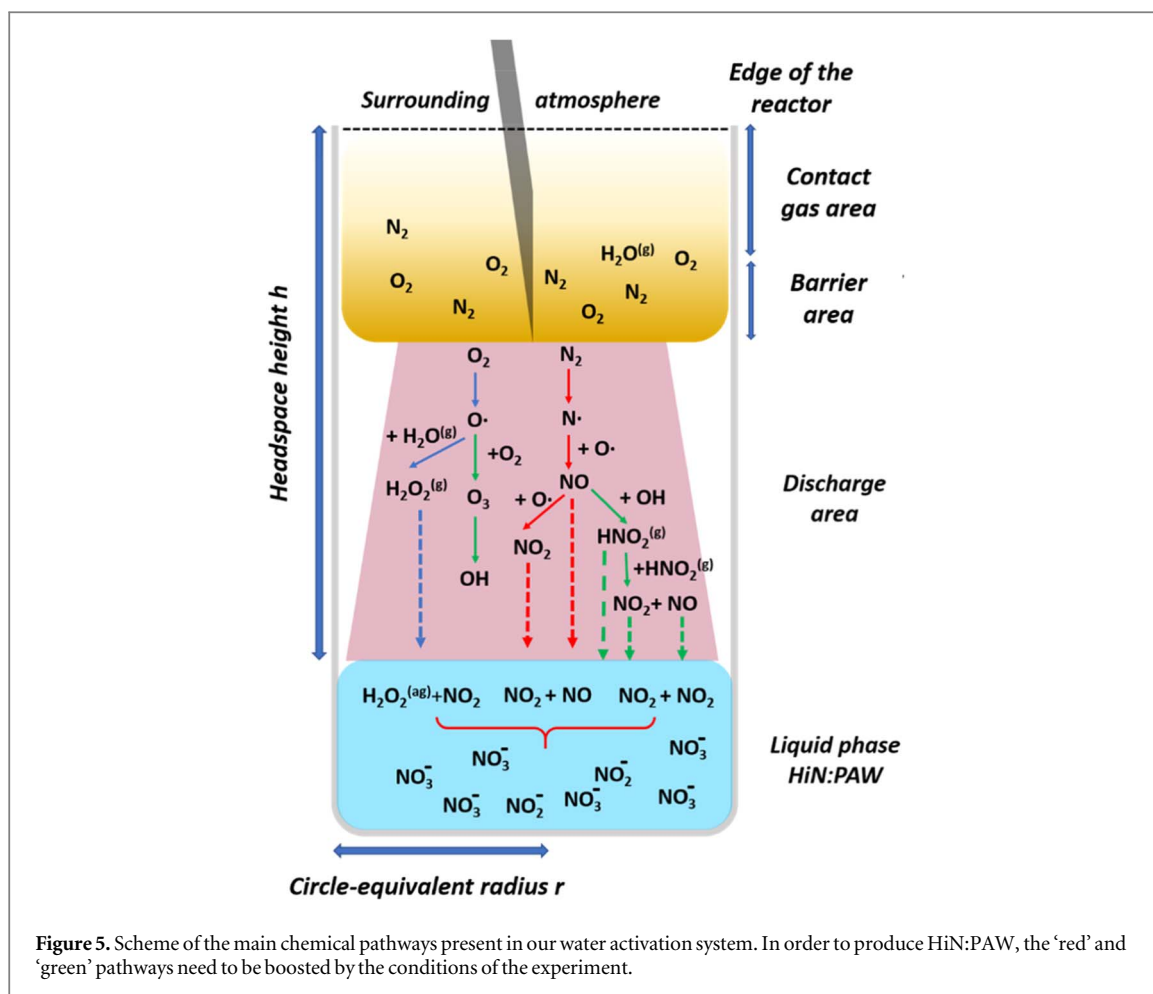
### 4.1. High-humidity environment

Despite serving as a general framework, equations (2a)–(2e) do not provide the mechanism of the high content of nitrogen-related species in HiN:PAW. Here, the detailed electrospaying experiments of transient spark discharge by Janda *et al* [20] have already demonstrated the importance of water humidity and HNO<sub>2</sub> in the process of producing PAW with high concentrations of NO<sub>x</sub><sup>-</sup>. They show that production of HNO<sub>2</sub> in the gas phase:



is an important chemical pathway. Henry's law coefficients  $k_H$  of HNO<sub>2</sub>, representing the solubility in water, of 50 mol kg<sup>-1</sup> atm<sup>-1</sup> at 300 K is four and five orders of magnitude higher than  $k_H^{\text{NO}_2} = 7 \times 10^{-3}$  mol kg<sup>-1</sup> atm<sup>-1</sup> and  $k_H^{\text{NO}} = 1.8 \times 10^{-3}$  mol kg<sup>-1</sup> atm<sup>-1</sup>, respectively. As a result of a much higher solubility of HNO<sub>2</sub> in water, HNO<sub>2</sub> itself is a significant source of nitrogen in HiN:PAW. Despite its lower concentration in the discharge area when compared to NO and NO<sub>2</sub>, HNO<sub>2</sub> can be quickly transferred into water in the form of NO<sub>2</sub>, either directly or by its solvation into potential microdroplets formed round the water/discharge interface [20]. HNO<sub>2</sub> and NO<sub>2</sub> are then the main sources of NO<sub>2</sub><sup>-</sup> and NO<sub>3</sub><sup>-</sup> in PAW:





Even though the mechanism of how the nitrogen-related species become dissolved in water are the same in our experiments, we are able to achieve analogical results using a much simpler setup than Janda *et al* [20]. Moreover, we reach much higher nitrogen to hydrogen peroxide ratios. Whereas in Janda *et al* the  $\text{NO}_2$  to  $\text{H}_2\text{O}_2$  ratio is around 40:1 in favour of  $\text{NO}_2$ , we obtained an even higher ratio of 140:1 and our HiN:PAW also contains high concentrations of  $\text{NO}_3^-$ , in the ratio of  $20 \times 10^3 : 1$  when compared to  $\text{H}_2\text{O}_2$ . Here, we have even improved on our previous results: [34] using the 1.5 ml volume of water in the Narrow container, the concentration of  $\text{NO}_3^-$  in PAW reached  $300 \text{ mmol l}^{-1}$ , which is more than 3 times higher than we obtained previously [34].

#### 4.2. Discharge conditions

Discharge properties also have a significant impact on the formation of HiN:PAW. The inability of non-pulse discharge to produce HiN:PAW even under otherwise favorable conditions had already been documented elsewhere [34]. Here, we showed that the effective dissociation of air molecules in the discharge is crucial. In particular, high concentrations of nitrogen and oxygen radicals need to be present (equations (2)). Based on our results (figure 3(D)), there are two opposite influences affecting the concentration of radicals: (i) the generation of the radicals in the discharge and (ii) their subsequent consumption by chemical reactions (reactions not leading to the formation of  $\text{NO}$  or  $\text{NO}_2$ , e.g. equation (2d)). While the increase of the peak current increases the concentration of the radicals, the prolongation of the pulse period gives the radicals more time to produce  $\text{H}_2\text{O}_2$ . As the increase of the ballast capacitance affects the two discharge parameters in an opposite way, there is an optimal combination (10.6 A and 390  $\mu\text{s}$ ).

Within the discharge area, we highlight three chemical pathways, as shown in figure 5: (i) the one resulting in  $\text{H}_2\text{O}_2$  (the blue path, equations (1b) and (2d)), (ii)  $\text{NO}$  and  $\text{NO}_2$  without  $\text{OH}$  (the red path, equations (1a), (2a, 2c)) and (iii)  $\text{NO}$  and  $\text{NO}_2$  through  $\text{OH}$  and  $\text{HNO}_2$  (the green path, equations (2b, 2e) and, (5a, 5b)). In standard PAW generation systems, the red and green pathways are significantly suppressed, resulting in PAW with high  $\text{H}_2\text{O}_2$  and a low amount of nitrogen-related radicals. In our system, it is just the opposite. To significantly increase the efficiency of red and green pathways, there needs to be a high concentration of nitrogen radicals. The concentration of  $\text{N}_2$  in air is clearly much higher than that of  $\text{O}_2$ , but  $\text{N}_2$  possesses a much higher

bond-dissociation energy (9.8 eV), in contrast to  $O_2$  (5.2 eV). Therefore, high-energy pulse discharge is necessary to effectively dissociate nitrogen molecules (optimized transient spark) and they need to be kept in the discharge region for some time to effectively accumulate - 10 min in our case (figures 3(C), (D) and 4(A)). Under such conditions, the oxygen radicals are consumed mainly in the red and green pathways, causing a decrease of  $H_2O_2$  and a high concentration of  $NO_2$  and  $NO$ . This scheme agrees with the observations presented in figure 3(E). The  $NO_2$ ,  $NO$  and  $HNO_2$  species are afterwards a source of an exceptionally high concentration of  $NO_2^-$  and  $NO_3^-$  in the resulting HiN:PAW, as described in section 4.1. Residual hydrogen peroxide in PAW is neutralized through equation (3).

#### 4.3. Gas-discharge intermediary phase

The discharge conditions favorable for the production of HiN:PAW are achieved only under certain reaction vessel geometries and volumes of water in the vessel, as reflected in the  $P$  and  $r_{max}$  parameters (figure 2(C)). To explain these results, we propose a model in which, in addition to the obvious liquid and discharge areas, the gas phase at the top part of the reactor is divided into two areas. While the upper one can effectively exchange molecules with the surrounding atmosphere (labelled as the *Contact gas area*), the lower part the gradient of the concentration of the relevant species effectively acts as a partial barrier between the surrounding atmosphere and the discharge area (labelled as the *Barrier area*). The presence of the barrier area limits the exchange of air molecules from the surrounding air with the discharge area and thus it allows the discharge to effectively dissociate the air molecules, especially  $N_2$ .

The importance of the formation of the gas-discharge intermediary area is illustrated by our experiments using different geometries in figures 2(A) and (C). Using a wide open vessel larger than the discharge itself  $r > r_{max}$  the outer atmosphere can to a large extent interfere with the discharge, bringing in more of the initial air-originating reactants ( $N_2$  and  $O_2$ ). Thus, the unrestricted air flow leads to the decrease in the concentration of reactive species above the water-discharge interface (equations (2a, 2c)). A higher but still not sufficient level of nitrogen-related species can be reached using a narrower ( $r < r_{max}$ ) reactor, see the  $P = 0.5$  conditions for the Medium vessel in figure 2(A). However, the best conditions were provided when the reaction vessel was 'tall', signifying that the vessel walls are high enough to form a semi-closed space for the plasma discharge, which leads to a more reactive environment. This situation occurs for higher barrier parameter values  $P > 1$ . Importantly, some air flow delivering the source  $N_2$  and  $O_2$  molecules is still necessary for the reactions to take place (see equations (1)), as we have already pointed out in our previous work [34]. Thus, a trade-off between the flow of the new source molecules and the formation of a highly reactive environment needs to be reached. Based on the results presented in figure 2(B), we propose that such a trade-off is reached for geometries close to, but above  $P = 1$  in figure 2(C).

Based on the analysis of the discharge presented in figures 3 and 4, the geometry of the activation process described by the  $P$  parameter influences not only the composition of the activated water, but also the concentration of  $NO_x$  in the discharge area. These experiments also give the timeframe, about 10 min, after which the composition of the activated water changes into the low  $H_2O_2$ /high nitrites and nitrates mode, in correspondence to the discharge with a high concentration of O and N atoms instead of the molecular signal. The same build-up time in the dynamics of the produced reactive species was observed for vessels with two different geometries, suggesting that in this case it is the geometry of the discharge itself which governs the dynamics of the activation process.

Our experiments confirm that a wide variety of parameters influence the production of HiN:PAW. Clearly, PAW is an extremely complex mixture of reactive species and possible reaction pathways, which need to be determined experimentally rather than predicted by theoretical calculations. Thus, for the time being, we formulate the conditions favorable for the production of HiN:PAW phenomenologically based on our experiments, without the quantification of the rates of the corresponding chemical equations, which are beyond the scope of the current work and topic for further research.

## 5. Conclusion

Based on the monitoring of the chemical composition of HiN:PAW, the emission spectroscopy of the used discharge and the chemical composition of discharge zone, we showed that a crucial condition for the production of HiN:PAW was an increase of air-originating atomic radicals in the discharge area, which was, in our experimental geometry, obtained after 10 min of the discharge burning. This condition of the discharge was enabled by the generation of a gradient of the concentration of the relevant species in the reaction vessel above the discharge, which effectively acts as a partial barrier limiting, but not completely preventing the air flow between the discharge area and the surrounding atmosphere. The formation of this barrier area and its influence on the outcome of the activation process can be very simply adjusted by the geometry of the activation process.

We describe this influence phenomenologically, using a barrier parameter  $P$  dependent on headspace height  $h$  and the effective radius of the vessel, while also noting the maximal effective vessel radius  $r_{\max}$  for the activation process to lead to HiN:PAW. The high concentration of atomic air radicals in the discharge resulting from an optimized  $P$  parameter subsequently boosted the chemical pathways leading to the increase in the concentration of nitrogen related species. In addition to  $\text{NO}_2$ , the production of  $\text{HNO}_2$  was an important pathway, because it readily solvates in water. The combination of these factors allowed us to reach PAW with the  $\text{NO}_3^-$  to  $\text{H}_2\text{O}_2$  ratio at least  $20 \times 10^3:1$ , in contrast to approximately 1:1 under more traditional conditions. These results thus show a way to robustly and reliably tune the dominant chemical pathways in a complex system of interconnected individual pathways taking place in plasma activated liquids by controlling a simple parameter of the overall geometry of the activation setup.

## Acknowledgments

This research was supported by the Czech Science Foundation Project GAČR GF21-39019L (JK, VS), GF23-05784S (FM, PG, KK).

## Data availability statement

The data generated and/or analysed during the current study are not publicly available for legal/ethical reasons but are available from the corresponding author on reasonable request.

## ORCID iDs

F Matějka  <https://orcid.org/0000-0003-3291-2242>

P Galář  <https://orcid.org/0000-0003-2220-2976>

V Scholtz  <https://orcid.org/0000-0002-6981-6169>

K Kúsová  <https://orcid.org/0000-0002-8545-5965>

## References

- [1] Bruggeman P J *et al* 2016 Plasma–liquid interactions: a review and roadmap *Plasma Sources Sci. Technol.* **25** 053002
- [2] Tendero C *et al* 2006 Atmospheric pressure plasmas: a review *Spectrochim. Acta, Part B* **61** 2–30
- [3] Ehlbeck J *et al* 2011 Low temperature atmospheric pressure plasma sources for microbial decontamination *J. Phys. D* **44** 13002
- [4] Fridman A, Gutsol A and Cho Y I 2007 Non-thermal atmospheric pressure plasma *Advances in Heat Transfer*, ed A Fridman *et al* (USA: Elsevier) **40**, 1–142
- [5] Sonawane S K, T M and Patil S 2020 Non-thermal plasma: an advanced technology for food industry *Food Science and Technology International* **26** 727–40
- [6] Magureanu M *et al* 2021 A review on non-thermal plasma treatment of water contaminated with antibiotics *J. Hazard. Mater.* **417** 125481
- [7] Šerá B *et al* 2021 Effects of non-thermal plasma treatment on seed germination and early growth of leguminous plants—a review **10** 1616
- [8] López M *et al* 2019 A review on non-thermal atmospheric plasma for food preservation: mode of action, determinants of effectiveness, and applications *Front. Microbiol.* **10** 622
- [9] Jeong W-S *et al* 2018 The effects of non-thermal atmospheric pressure plasma treated titanium surface on behaviors of oral soft tissue cells *Sci. Rep.* **8** 15963
- [10] Scholtz V *et al* 2015 Nonthermal plasma — a tool for decontamination and disinfection *Biotechnol. Adv.* **33** 1108–19
- [11] Randeniya L K and de Groot G J J B 2015 Non-thermal plasma treatment of agricultural seeds for stimulation of germination, removal of surface contamination and other benefits: a review **12** 608–23
- [12] Julák J *et al* 2018 Contribution to the chemistry of plasma-activated water *Plasma Phys. Rep.* **44** 125–36
- [13] Thirumdas R *et al* 2018 Plasma activated water (PAW): chemistry, physico-chemical properties, applications in food and agriculture *Trends in Food Science and Technology* **77** 21–31
- [14] Ashford B and Tu X 2017 Non-thermal plasma technology for the conversion of  $\text{CO}_2$  *Current Opinion in Green and Sustainable Chemistry* **3** 45–9
- [15] Geyter N D and Morent R 2012 Nonthermal plasma sterilization of living and nonliving surfaces 14255–74 *Annual Review of Biomedical Engineering* **14** 255–74
- [16] Obrová K *et al* 2022 Decontamination of high-efficiency mask filters from respiratory pathogens including SARS-CoV-2 by non-thermal plasma *Front. Bioeng. Biotechnol.* **10** 815393
- [17] Kovačević V V *et al* 2022 Low-temperature plasmas in contact with liquids—a review of recent progress and challenges *J. Phys. D* **55** 473002
- [18] Mariotti D *et al* 2012 Silicon nanocrystals in liquid media: optical properties and surface stabilization by microplasma-induced non-equilibrium liquid chemistry *Advanced Functional Materials* **22** 954–64
- [19] Magureanu M *et al* 2013 Toluene oxidation by non-thermal plasma combined with palladium catalysts *Front. Chem.* **1** 7
- [20] Janda M *et al* 2021 The role of  $\text{HNO}_2$  in the generation of plasma-activated water by air transient spark discharge **11** 7053
- [21] Ganesh Subramanian P S *et al* 2019 Characterization of plasma activated water for medical applications *Adv. Mater. Res.* **10** 919–23

- [22] Zhou R *et al* 2020 Plasma-activated water: generation, origin of reactive species and biological applications *J. Phys. D* **53** 303001
- [23] Bradu C *et al* 2020 Reactive nitrogen species in plasma-activated water: generation, chemistry and application in agriculture *J. Phys. D* **53** 223001
- [24] Machala Z *et al* 2013 Formation of ROS and RNS in water electro-sprayed through transient spark discharge in air and their bactericidal effects *Plasma Process. Polym.* **10** 649–59
- [25] Cheng H *et al* 2022 On the dose of plasma medicine: plasma-activated medium (PAM) and its effect on cell viability *Phys. Plasmas* **29** 063506
- [26] Mazzaro R, Romano F and Ceroni P 2017 Long-lived luminescence of silicon nanocrystals: from principles to applications *Phys. Chem. Chem. Phys.* **19** 26507–26
- [27] Kovalenko M V *et al* 2015 Prospects of nanoscience with nanocrystals *ACS Nano* **9** 1012–57
- [28] Dohnalová K, Gregorkiewicz T and Kůsová K 2014 Silicon quantum dots: surface matters *J. Phys. Condens. Matter* **26** 173201
- [29] Mobarok M H *et al* 2017 Instantaneous functionalization of chemically etched silicon nanocrystal surfaces *Angewandte Chemie - International Edition* **56** 6073–7
- [30] van den Boom A F J *et al* 2020 Fast room-temperature functionalization of silicon nanoparticles using alkyl silanols *Faraday Discuss.* **222** 82–94
- [31] Yu Y *et al* 2013 Room temperature hydrosilylation of silicon nanocrystals with bifunctional terminal alkenes *Langmuir* **29** 1533–40
- [32] Galář P *et al* 2017 Influence of non-thermal plasma on structural and electrical properties of globular and nanostructured conductive polymer polypyrrole in water suspension *Sci. Rep.* **7** 15068
- [33] Tyler B J 1962 Reaction of hydrogen peroxide and nitric oxide *Nature* **195** 279–80
- [34] Galář P *et al* 2021 Non-thermal pulsed plasma activated water: environmentally friendly way for efficient surface modification of semiconductor nanoparticles *Green Chem.* **23** 898–911
- [35] Khun J *et al* 2018 Various DC-driven point-to-plane discharges as non-thermal plasma sources and their bactericidal effects *Plasma Sources Sci. Technol.* **27** 065002
- [36] Hozák P *et al* 2018 Further contribution to the chemistry of plasma-activated water: influence on bacteria in planktonic and biofilm forms *Plasma Phys. Rep.* **44** 799–804